

Performance of vacuum-insulated central pipes for deep borehole heat exchangers in geothermal systems

Ján Kubačka^{1,2} , Tassos G. Karayiannis^{3,*} 

¹Faculty of Mechanical Engineering, Energy Institute, Brno University of Technology, Technická 2896/2, 61669 Brno, Czech Republic

²GA Drilling, a. s., Vápenka 4, 84107 Bratislava, Slovak Republic

³Centre for Energy Efficient and Sustainable Technologies, Department of Mechanical and Aerospace Engineering, Brunel University London, Kingston Lane, Uxbridge UB8 3PH, UK

*Corresponding author. Centre for Energy Efficient and Sustainable Technologies, Department of Mechanical and Aerospace Engineering, Brunel University London, Kingston Lane, Uxbridge UB8 3PH, UK. E-mail: tassos.karayiannis@brunel.ac.uk

Abstract

Geothermal energy is considered a promising future energy prospect, with the geothermal well outlet temperature being one of the important parameters affecting possible utilization options. For ground source heat pump applications or direct district heating, using lower temperatures can be acceptable. However, efficient electricity production requires a higher enthalpy gradient, which cannot be achieved without high temperature at the wellhead. The selection of the dry co-axial close-loop deep borehole systems (DBHE) may be, in some cases, very beneficial. The operating performance of co-axial DBHE can be optimized if the undesired heat transfer between the central pipe and annular fluid zones is minimized. Therefore, the operational performance of such a system depends strongly on the high thermal resistance of the central pipe. The most common option would be a low thermal conductivity material, such as high-density polyethylene (HDPE). In addition, vacuum-insulated tubing (VIT) used as the central pipe could be considered. The article presents results from the study aimed at the comparison of the homogeneous central pipe made of HDPE material and the gap-insulated central pipe. In the study, various air pressure levels as well as variations of surface emissivity were examined to reveal the effect on the heat transfer between the fluid channels. The simulation has been performed using a new purposely developed WellTH simulation software. A coaxial heat exchanger system using a VIT outperforms significantly the heat exchanger with an HDPE for deep geothermal wells. However, this advantage diminishes for shallow wells and therefore this tendency should be considered in the design stage.

Keywords: geothermal energy; co-axial heat exchanger; closed-loop system; vacuum-insulated central pipe

1 Nomenclature

- a = thermal diffusivity [m^2/s]
- A = heat transfer surface area [m^2]
- A_{flow} = flow area (m^2)
- c_p = specific heat capacity [$\text{J}/\text{kg K}$]
- d = particle diameter [m]
- D_h = hydraulic diameter [m]
- dl = length of the element [m]
- E_1 = exponential integral
- f = Darcy friction factor [–]
- g = acceleration due to gravity (9.81) [m/s^2]
- G_{grad} = geothermal gradient [$^\circ\text{C}/\text{km}$]
- Gr = Grashof number [–]
- h = heat transfer coefficient [$\text{W}/\text{m}^2 \text{K}$]
- k = thermal conductivity [$\text{W}/\text{m.K}$]
- k_B = Boltzmann constant ($1.381e^{-23}$) [J/K]
- Kn = Knudsen number [–]
- l = mean free path [m]
- L = length [m]
- L_{ch} = characteristic length [m]
- lpm = liters per minute
- M = molar mass [kg/mol]
- MF = molecular flow
- \dot{m} = mass flow rate [kg/s]
- n = number of elements [–]
- Nu = Nusselt number [–]
- p = pressure [Pa]

- P = pumping power [W]
- Pr = Prandtl number [–]
- q = rate of heat flow per element length [W/m]
- \dot{Q}_i = rate of heat flow [W]
- r = radial coordinate [m]
- R = thermal resistance (K/W)
- R_o = universal gas constant [$\text{J}/\text{K.mol}$]
- Ra = Rayleigh number [–]
- Re = Reynolds number [–]
- SF = slip flow
- SR = absolute roughness of the surface [m]
- T = temperature [K]
- TF = transitional flow
- u = dummy variable
- v = flow velocity [m/s]
- V = volume [m^3]
- WP = wetted perimeter [m]

Greek Letters

- β = thermal expansion coefficient [$1/\text{K}$]
- Δ = gradient [–]
- ε = surface emissivity [m]
- η = pump efficiency
- μ = dynamic viscosity [Pa.s]
- ν = kinematic viscosity [m^2/s]
- π = mathematical constant
- ρ = density [kg/m^3]

Received 30 April 2024; revised 15 June 2024; accepted 18 June 2024

© The Author(s) 2024. Published by Oxford University Press.

This is an Open Access article distributed under the terms of the Creative Commons Attribution License (<http://creativecommons.org/licenses/by/4.0/>), which permits unrestricted reuse, distribution, and reproduction in any medium, provided the original work is properly cited.

- σ = Stefan Boltzmann constant ($5.67e-8$) [$W/m^2 \cdot K^4$]
- τ = time [s]

Subscripts

- 1 = inner surface of air gap layer
- 2 = outer surface of air gap layer
- 0 = standard atmospheric conditions
- a = annulus
- air = air property
- b = borehole
- c = central pipe
- f = fluid
- g = ground
- inf = influence
- ins = insulation
- int, ext = internal, external
- L, T, P = laminar, turbulent, transitional
- rad = radiative term
- s = surface
- $surf$ = earth's surface
- ∞ = far-field

1 Introduction

The detrimental environmental effects of past and present broad use of fossil fuels are widely acknowledged, and it is more than obvious that mankind is entering a new era of carbon-free energy sources. The need for a clean energy use prioritization appears to be inevitable and highly necessary. It is well known that geothermal energy has a significant potential to contribute to an energy mix as it can provide relatively clean baseload energy. The majority of geothermal systems that operate nowadays are classified as open. The open systems are set up to retrieve heat from the hot water aquifer found at specific depths. However, the availability of these aquifers represents a significant constraint. They may not be located at a place where the heat can be effectively utilized, and even if they are, the parameters of retrieved water may not be sufficient for convenient and effective use. The current state of drilling technology enables the creation of artificial aquifers but at the cost of the possible occurrence of seismic events. This may somehow limit the use of such techniques in the vicinity of populated areas where the geothermal heat would have been most likely used. Another limitation in open systems, where a fluid is injected in one of the loops and retrieved in a second loop, would be rock permeability or porosity. The closed systems, on the contrary, do not rely on the presence of such aquifers or the level of rock permeability and hence can easily be deployed worldwide [1]. Another aspect to consider would be installation costs. The drilling process contributes up to 50% of the total costs of the geothermal plant [2]. This is a significant portion and hence the idea of repurposing existing old oil and gas wells has become very appealing in recent years. Nowadays, there are thousands of abandoned wells all over the world [3–5]. The above, namely the elimination of possible seismic events and soil subsistence, the possibility of locating the well near where the thermal energy is needed, the need for only a single well and hence the possibility of repurposing existing oil and gas wells, plus reduced corrosion and fouling see also Alimonti and Soldo [6], could favour the establishment of single closed-loop co-axial systems, even though their performance may be lower compared to an open-loop system.

The operational performance of the coaxial DBHE system for specific locations in a wellbore trajectory depends on the ability of the rock formation to transfer the heat from the distance of the wellbore and by the level of parasitic heat transfer between the central pipe (outflow) and annular (inflow) fluid zones. The ability of the rock to conduct heat is characterized by its thermophysical properties and cannot be improved. What can be improved, on the other hand, is the rate of heat flow between two adjacent fluid zones. Minimization of this heat transfer rate would lead to higher efficiency of the system. The problem is exacerbated by the fact that there is not much space inside the wellbore. The central pipe dimensions must be carefully selected also in terms of the flow pressure drop that affects the pumping power, which subsequently affects the economy of the system. Another option would be the selection of a low thermal conductivity material or a specific vacuum, or air gap insulated central pipe. Over time, several central pipe materials and designs have been considered for the DBHE applications. The most important ones are summarized by Śliwa *et al.* [7] as follows:

- A simple steel central pipe.
- A simple composite or polymer central pipe.
- Steel central pipe with an insulation layer.
- Double steel central pipe with insulation fluid.
- Vacuum insulated tubing (VIT).

The main asset of the simple steel central pipe would be its accessibility. The standard drill pipes or coiled-tubing pipes could be easily found on the market and are also relatively cheap. The installation procedure is, however, rather complicated due to the weight of the system. The biggest disadvantage comes with the thermal conductivity of the steel which is much higher than, for instance, the composite or polymer material. The use of composite materials, such as fiberglass, or polymer materials, such as polyethylene or polypropylene appears to be a much better option. These are commonly accessible on the market, have low thermal conductivity, low weight, and installation is much easier. For instance, the high-density polyethylene (HDPE) pipes can be welded directly on-site just before running into a hole. On the other hand, the temperature limitation ($80^\circ C$) could be a limiting factor and may prevent them from being used in deep geothermal systems. The thermal resistance of the steel pipe can be enhanced when using an additive insulation layer. Most of the off-the-shelf products come with an external layer of polyurethane foam, which is covered by a protective plastic layer. Polyurethane foam provides very good thermal resistance, and some polyurethane chemistries are stable at higher temperatures (up to $150^\circ C$). The major disadvantage of this solution lies in its fragility. The protective plastic layer must remain intact throughout the entire installation process and during the operation of the DBHE system. Any loss of integrity would lead to water incursion and destroy its insulation ability. The last two on the list above are based on a similar design. The central pipe consists of two concentric steel tubings and the high thermal resistance of the system is secured by the gap in between the two. The gap could be filled with insulation fluid, such as air or nitrogen or there is a vacuum that effectively minimizes heat transfer across the central pipe. There is an extensive list of vacuum tubing suppliers providing the vacuum-insulated tubing (VIT) system. All of them provide coaxial

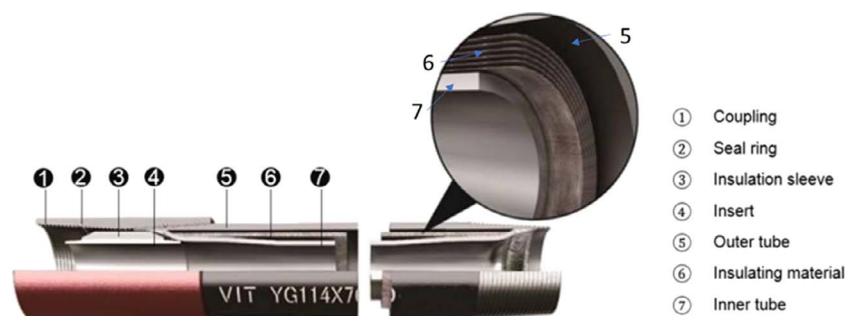


Figure 1. Design of the VIT, adapted from [8].

vacuum-insulated pipes that can be further assembled into the central pipe.

Originally, VIT systems have been designed for enhanced oil recovery operations. VIT systems are also often used to prevent annular pressure build-up in deep water completions in wells with no access to the casing annuli, wax depositions, wellbore thawing in permafrost zones and can also mitigate the formation of the methane gas hydrates during well shut-down and cold start-up of the production operations. The last research activities in the field of DBHE indicate that the use of VIT could be beneficial also for the geothermal industry.

The purpose of this article is to provide an assessment of the gap-insulated central pipe system for the DBHE application in comparison to the homogeneous central pipe made of HDPE material. Attention is paid to the variation of the air gap pressure level and central pipe surface emissivity to determine the effect of both on the thermal response of the DBHE. In addition, the effect of different DBHE lengths is also assessed. The final discussion is related to the optimization of the fluid flow rate to achieve maximal outlet temperature at the wellhead.

2 Design of the VIT

From a high-level perspective, the VIT consists of two coaxial steel tubings, see Fig. 1 from [8]. The free volume between the two is kept at low pressure which ensures negligible convective/conductive heat transfer through the gap. The inner surface of the tubing usually contains aluminium foil layers separated by non-conductive material called scrim. The aluminium foil is characterized by a very low surface emissivity, which significantly decreases radiative heat transfer within the VIT. The low-pressure level is achieved during the VIT manufacturing process using a vacuum pump and further maintained using a chemical pump called a getter throughout the entire lifespan. The use of a getter is essential as it prevents continuous hydrogen gas pressure build-up because of pipe corrosion in an adverse wellbore environment. Data retrieved from the Peace River oil field provided by Cormier [9] indicate a steep hydrogen build-up in the VIT annular zone in one year of continuous operation in systems without a hydrogen getter. As mentioned above, the presence of low gas pressure is important, as it decreases the conductive term within the VIT. An absolute value of gas pressure of ~ 10 Pa has been documented in references [10, 11]. Another fact that is important to mention is that hydrogen has much higher thermal conductivity than air and its temperature dependency is steeper. To avoid such problems, non-vacuum insulated tubings are also being considered for future applications [12].

2.1 Heat losses: the overview

The thermal performance of the VIT systems is usually rated using the physical quantity of thermal conductivity or sometimes by the term apparent thermal conductivity. It has been noted [11] that the widely used simplistic 1D heat transfer approach has its limitations due to the 3D nature of the heat flow. Study shows that there is a significant amount of heat transfer around the coupler and weld zones. In addition, the hot zone around the coupler is usually extended by 0.3 to 0.6 m in the axial direction and hence the VIT structure behaves as a 2D axisymmetric fin. The rate of heat being transferred in the axial direction also depends on the boundary conditions. The apparent thermal conductivity would vary at different boundary conditions, such as heat transfer described by the Stefan–Boltzmann law exhibits non-linear behaviour in terms of the boundary temperatures. To conclude, the proper thermal–hydraulic assessment of the standard-of-the-shelf VIT system would require a complex 3D modeling approach. In this study, we will assume the VIT to be a continuous system of two concentric pipes with no couplers. The actual proportional change due to different higher heat transfer rates at the couplers will be included in a later study.

2.1 2.2. Air gap thermal conductivity

The presence of low-pressure gas in the annular region of the VIT significantly affects the thermal conductivity of the system. If the ideal vacuum in the system is maintained, the conductive term of the heat transfer can be omitted. However, it has been reported that only a medium vacuum level is generally achieved and maintained during the manufacturing process, [10, 11]. To evaluate the impact of the presence of the low-gas environment on the conductive heat transfer, the selection of a proper formulation of the fluid dynamics should be conducted using the Knudsen number Kn , given by Equation (1).

$$Kn = \frac{l}{L_{ch}} \quad (1)$$

The characteristic length of the system refers to the size of the gap. The mean free path refers to the average distance that a moving particle travels before experiencing a significant change in its trajectory or energy. Such a change is often due to successive collisions with other particles. It can be calculated as follows [13]:

$$l = \frac{k_B T}{\sqrt{2} \pi d^2 p} \quad (2)$$

Table 1. Knudsen number as a function of pressure and temperature.

		Temperature [°C]							
		20	40	60	80	100	120	140	160
Pressure [Pa]	1.0E-02	8.2E+01	8.8E+01	9.4E+01	9.9E+01	1.1E+02	1.1E+02	1.2E+02	1.2E+02
	1.0E-01	8.2E+00	8.8E+00	9.4E+00	9.9E+00	1.1E+01	1.1E+01	1.2E+01	1.2E+01
	1.0E+00	8.2E-01	8.8E-01	9.4E-01	9.9E-01	1.1E+00	1.1E+00	1.2E+00	1.2E+00
	1.0E+01	8.2E-02	8.8E-02	9.4E-02	9.9E-02	1.1E-01	1.1E-01	1.2E-01	1.2E-01
	1.0E+02	8.2E-03	8.8E-03	9.4E-03	9.9E-03	1.1E-02	1.1E-02	1.2E-02	1.2E-02
	1.0E+03	8.2E-04	8.8E-04	9.4E-04	9.9E-04	1.1E-03	1.1E-03	1.2E-03	1.2E-03
	1.0E+04	8.2E-05	8.8E-05	9.4E-05	9.9E-05	1.1E-04	1.1E-04	1.2E-04	1.2E-04
	1.0E+05	8.2E-06	8.8E-06	9.4E-06	9.9E-06	1.1E-05	1.1E-05	1.2E-05	1.2E-05

Table 2. Thermal conductivity coefficient $k(p)/k_0$ as a function of pressure and temperature for a gap size of 8.51 mm

		Temperature [°C]							
		20	40	60	80	100	120	140	160
Pressure [Pa]	1.0E-02	0.004	0.004	0.003	0.003	0.003	0.003	0.002	0.002
	1.0E-01	0.039	0.035	0.033	0.030	0.028	0.026	0.025	0.023
	1.0E+00	0.283	0.269	0.257	0.245	0.235	0.225	0.216	0.207
	1.0E+01	0.791	0.780	0.769	0.759	0.750	0.741	0.732	0.723
	1.0E+02	0.974	0.973	0.971	0.969	0.968	0.966	0.964	0.962
	1.0E+03	0.997	0.997	0.997	0.997	0.997	0.996	0.996	0.996
	1.0E+04	1.000	1.000	1.000	1.000	1.000	1.000	1.000	1.000
	1.0E+05	1.000	1.000	1.000	1.000	1.000	1.000	1.000	1.000

If the mean free path of the molecule reaches the size of the length scale of the domain, the continuum mechanics formulation of the fluid dynamics is not an appropriate selection for the problem description and instead, the statistical mechanics should be used. In such a case, the thermal conductivity of the fluid is no longer a parameter that solely relates to a certain material under specific conditions, but it also depends on the size of the domain. As described in [14], the classification of the flow regime has been slightly changing over time, yet has settled as follows:

- $Kn < 0.01$ Continuum flow.
- $0.01 < Kn < 0.1$ Slip flow.
- $0.1 < Kn < 10$ Transitional flow.
- $Kn > 10$ Free molecular flow.

The average particle diameter for the air mixture would be calculated as 0.360 nm, i.e. based on the mole fraction weighted average of oxygen and nitrogen molecular diameters, taken here as 0.346 nm and 0.364 nm, respectively [15]. Let the gap size for the future analysis be 8.51 mm. The values of Knudsen number as a function of the pressure and temperature in the VIT are summarized in Table 1. Based on the values in the table, it can be stated that for pressures above 100 Pa continuum flow should be considered. The slip flow regime would provide the best fit for pressures around 10 Pa. The transitional flow regime should be used to address a pressure level of ~ 1 Pa and a free molecular flow regime would be the best choice for a pressure level of ~ 0.1 Pa or less.

Tome [16] suggested equations for the calculation of a thermal conductivity coefficient $k(p)/k_0$ for slip flow SF and free molecular flow MF. After conversion into the SI units,

these are, respectively, as follows:

$$\left(\frac{k(p)}{k_0}\right)_{SF} = \frac{1}{1 + 7.657e - 5 \frac{T}{p L_{ch}}} \quad (3)$$

$$\left(\frac{k(p)}{k_0}\right)_{MF} = 20.264 \sqrt{T} \frac{p L_{ch}}{T k_0} \quad (4)$$

It can be shown that the data for the thermal conductivity coefficient in the transitional flow regime, TF, does not significantly differ (Kubačka J, 2024, unpublished data). Hence, a simple Knudsen number weighted average linear approximation can be carried out.

$$\left(\frac{k(p)}{k_0}\right)_{TF} = \frac{Kn - 0.1}{9.9} \left(\frac{k(p)}{k_0}\right)_{MF} + \left(1 - \frac{Kn - 0.1}{9.9}\right) \left(\frac{k(p)}{k_0}\right)_{SF} \quad (5)$$

The data obtained are shown in Table 2. Note that the formulation for the slip flow was used also for the continuum flow regime as it provides reasonable results.

The resulting data indicate that the pressure level of ~ 10 Pa, which is a typical pressure level (see [11]) is not sufficient for thermal insulation of the central pipe in terms of conductive heat transfer. The thermal conductivity of the air in the gap reaches 72–79% of the reference value at standard atmospheric conditions depending on gas temperature. For lower thermal conductivity of the air gap either lower gas pressures must be achieved and maintained, or the gap size must be significantly reduced. It can be seen from Equation (1) that the decrease of gap size by an order of magnitude would increase Kn at an identical rate.

Table 3. Rayleigh number as a function of pressure and temperature.

	Temperature [°C]								
	20	40	60	80	100	120	140	160	
Pressure [Pa]	1.0E+01	3.96E-05	2.97E-05	2.27E-05	1.76E-05	1.39E-05	1.11E-05	9.03E-06	7.41E-06
	1.0E+02	3.22E-03	2.38E-03	1.79E-03	1.38E-03	1.08E-03	8.52E-04	6.83E-04	5.54E-04
	1.0E+03	3.14E-01	2.32E-01	1.75E-01	1.34E-01	1.04E-01	8.26E-02	6.61E-02	5.36E-02
	1.0E+04	3.14E+01	2.31E+01	1.74E+01	1.34E+01	1.04E+01	8.23E+00	6.59E+00	5.34E+00
	1.0E+05	3.14E+03	2.31E+03	1.74E+03	1.34E+03	1.04E+03	8.23E+02	6.58E+02	5.33E+02

2.1 2.3. Natural circulation within the gap

Natural or free convection typically occurs in the continuum flow regime ($Kn < 0.01$). In such a regime, the mean free path of gas molecules is significantly smaller than the characteristic length scale of the flow. In slip flow, transitional flow, or free molecular flow regimes, the gas tends to deviate from the continuum assumptions in the traditional sense. Although evaluation of the natural circulation may not be necessary, it could be interesting to reveal the behaviour of the gas at higher pressures and see if any conclusion could be taken also for lower pressure levels. While the free molecular flow is described using statistical mechanics, the slip flow and transitional flow may also exhibit some characteristics related to the continuum flow. It has already been found that the regime within the VIT for a given gap size (8.51 mm) and pressure level (10 Pa) can be either characterized as slip flow or transitional flow for elevated temperatures. In addition, determining whether an increase in pressure (by an order of magnitude) would not promote natural circulation within the VIT system would also be beneficial.

In continuum mechanics formulation of fluid dynamics, the Rayleigh number, Ra , is a dimensionless parameter related to the buoyancy-driven flow. The Ra number can be expressed as the multiplication of the Grashof number Gr and Prandtl number Pr and can be calculated as follows:

$$Ra = Gr Pr = \frac{g \beta (T_s - T_\infty) L_{ch}^3 c_p \rho}{\nu k} \quad (6)$$

The Rayleigh number is the key parameter in the characterization of the nature of a flow and imposes a critical threshold. If the value of Ra drops below a certain value, the heat transfer occurs primarily through conduction and the presence of natural circulation is either insignificant or has practically no effect on overall heat transfer. The critical value of Ra is specific for a given geometry; however, it is in order of magnitude of 10^3 – 10^4 , [13]. The solution of Equation (6) can be significantly simplified when using the ideal gas approximation. At low temperatures, the gas molecules are widely spaced, intermolecular forces are negligible, and interactions between them are rare. The choice of the ideal gas model is thus appropriate for rarefied gases, except those at very low temperatures, which is not the case here. The thermal expansion coefficient, for the assumption of an ideal gas, can be given as $\beta = 1/T$. Geiser and Goldthwaite [17] experimentally confirmed that the dynamic viscosity, μ , of air does not change with decreasing pressure down to ~ 6 Pa. On the other hand, the kinematic viscosity, ν , does depend on pressure as it is calculated as $\nu = \mu/\rho$. Calculation of ideal gas

density can be performed using the equation of state:

$$\rho = \frac{p M_{air}}{R_o T} \quad (7)$$

The variation of specific heat capacity with pressure can be through the Maxwell relations [18] written here as follows:

$$\left(\frac{\partial c_p}{\partial p} \right)_T = -T \left(\frac{\partial^2 V}{\partial T^2} \right)_p \quad (8)$$

Substituting V using the ideal gas notation ($V = nR_o T/p$) can be easily lead to the fact that the second derivative of volume with temperature equals zero and thus, the specific heat capacity does not change with pressure.

For the Rayleigh number quantification, let's assume L_{ch} is equal to the size of the gap (8.51 mm) and the temperature difference ($T_s - T_\infty$) conservatively be 50°C . The results are included in Table 3.

It should be stated at this stage that the above calculation is an approximation since there is no empirical model dedicated to Ra calculation in the vertically oriented annular geometry and instead, a simple infinite wall slab approach was used [13]. However, it provides a relatively good indication that the geometry restricts free convection at low pressures. Even if there will be a slight increase in pressure during the VIT operation, no convective flow should be expected.

2.1 2.4. Radiative heat transfer

The heat transfer in the ideal vacuum system is solely driven by the radiative term, \dot{Q}_{rad} , calculated using the Stefan-Boltzmann law, see Equation (9). Unlike in conductive heat transfer, the rate of heat being transferred does not simply depend on the temperature gradient and exhibits strongly non-linear behaviour. It can hence be claimed that the system would behave differently at elevated temperatures even for the same temperature gradients. Consequently, the laboratory experiments at close-to-normal conditions may significantly underestimate the rate of heat flow compared to the real downhole environment. It is also important to note that surface emissivity has a decisive impact on the radiative term.

$$\dot{Q}_{rad} = \frac{\sigma A_1 (T_1^4 - T_2^4)}{\frac{1}{\varepsilon_1} + \frac{1-\varepsilon_2}{\varepsilon_2} \frac{r_1}{r_2}} = h_{rad} A_1 (T_1 - T_2) \quad (9)$$

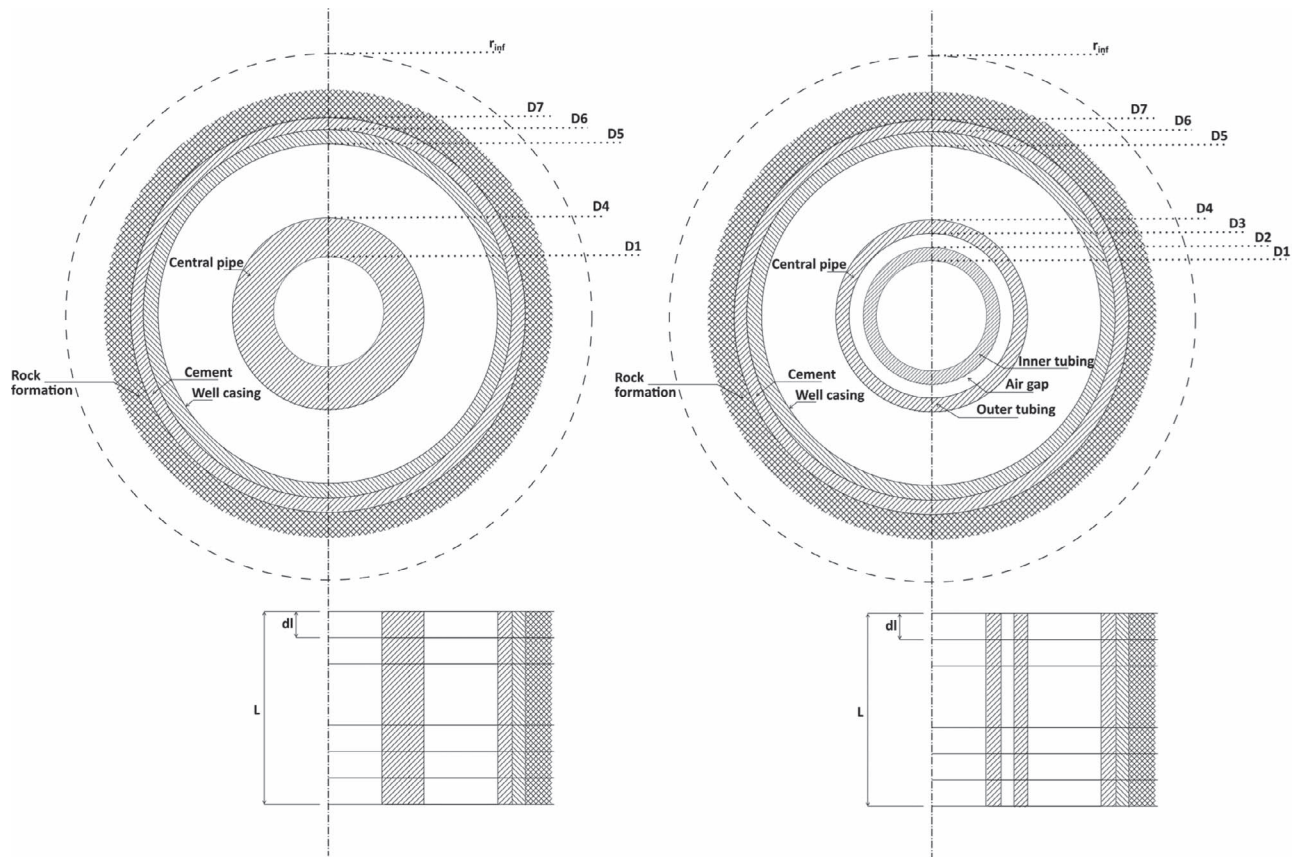


Figure 2. Outline of the DBHE geometry, HDPE (left), VIT (right).

The heat transfer coefficient for the radiative heat transfer term can be expressed using the following equation.

$$h_{\text{rad}} = \frac{\sigma (T_1^2 + T_2^2) (T_1 + T_2)}{\frac{1}{\epsilon_1} + \frac{1-\epsilon_2}{\epsilon_2} \frac{r_1}{r_2}} \quad (10)$$

In summary, at this point, a thorough computational assessment of the VIT heat losses requires complete design specification and most probably a computational fluid dynamics (CFD) simulation software. As mentioned above, Azzola *et al.* [11] report, that the heat losses around the coupler can be significant and the VIT pipe should then be, from the computational point of view, treated as an axisymmetric fin. In addition, the stand-alone simulation of one VIT pipe would not yield realistic results as these depend on the wellbore conditions as well. On the other hand, the use of the CFD approach would be for the geometry of such extent very time-demanding and nearly impossible. A simplified 1D approach applied to the standard VIT pipe geometry would be accepted as a good approximation.

It has been found that the vacuum level in the standard VIT pipes (~10 Pa) appears to be unsatisfactory when it comes to the decrease of thermal conductivity of the low-pressure gas layer. Effective thermal conductivity is not solely a material parameter in a low-pressure environment, but it also depends on the geometry of the system. For the 8.51 mm gap size and 10 Pa, the thermal conductivity of the air yields 72–79% of the reference value at standard atmospheric conditions depending on the temperature. Technically, the thermal conductivity

Table 4. DBHE geometry.

	Diameter [mm]	
	HDPE	VIT
D1	88.30	88.30
D2	–	101.60
D3	–	118.62
D4	139.70	139.70
D5	177.80	177.80
D6	198.52	198.52
D7	215.90	215.90

can be further reduced by lowering the pressure level or by decreasing the gap size. Implementation of the second option would, however, also reduce insulation thickness and hence adversely affect the thermal resistance of the pipe. It can also be concluded that the presence of a low-pressure environment inhibits natural convection in the air gap. The likelihood of this occurrence rises when the gap pressure approaches atmospheric levels, although the gap size also exerts a significant influence on this phenomenon.

3 Problem definition

Heat transfer in the close environment of the wellbore is described by the Fourier heat transfer equation. The Fourier equation, being a second-order partial differential equation, requires the specification of an initial condition and two boundary conditions to obtain a unique solution. However, the definition of both boundary conditions could be problematic. Employing the standard naming convention, the inner

Table 5. Material properties of solids.

	Density (kg/m ³)	Specific heat capacity (J/kgK)	Thermal conductivity (W/mK)
Steel	-	-	45.0
Cement	-	-	1.1
HDPE	-	-	0.54
Air	-	-	As per case examined
Rock	2750	800	2.5

surface of the external wellbore pipe can be represented by the boundary condition of the third kind (Robin – convective boundary condition). The far-field undisturbed thermal condition in the surrounding rock structures can be represented by the first-kind boundary condition (Dirichlet – fixed temperature). However, the wellbore far-field temperature is a function of the geothermal gradient and the position of this boundary is not implicitly defined. Figure 2 and Table 4 include the two geometries that are used in this study and the corresponding diameters respectively. The properties of the ground are given in Table 5.

Water has been selected as a heat carrier. The thermo-physical properties were taken from the NIST database [19] while the temperature dependency of these was preserved. The material properties of solids are provided in Table 5. Note that the thermal conductivity of the air gap is defined for each case separately. The absolute surface roughness of HDPE is set to 0.01 mm (smaller values are actually recommended, e.g. 0.0015 for HDPE but this conservative value is used) and for the steel tubing it is 0.05 mm, see [20, 21]. The surface emissivity of the steel varies from 0.03 when aluminium foil is used to 0.95 for bare material.

The heat transfer problem has a transient nature and there are several ways how it can be solved. The most convenient ones, among the others, would be using the implementation of the full transient numerical solution over a discretized domain or utilization of the approximate analytical solution. The first option requires the generation of a computational mesh and the transformation of the heat transfer differential equation into a set of algebraic equations solved for each element of the mesh separately. The specification of the far-field boundary position does not constitute any specific problem except that the size of the computational domain must be large enough to keep the volume affected by the temperature variation inside it during the entire simulation process. In other words, the heat wave propagation should not affect the temperature at the very last element of the computational mesh. The challenge with a complete numerical solution lies in the potential for demanding simulation run times and its complexity. Contrary to this, the approximate analytical solution of the heat transfer equation is much less time-consuming. The wellbore environment is treated as a semi-infinite body and the simulation uses a so-called quasi-steady-state assumption. The analytical solution requires a firm specification of the right boundary position whereas it has been proved, that such position varies with the elapsed time of the DBHE operation.

A pioneering work in this field was based on Kelvin's theory of heat sources and can be attributed to Carslaw and Jaeger [22]. They proposed a mathematical construction of two cornerstone analytical models widely used even today, an infinite line-source model and the infinite cylindrical-

source model. The infinite cylindrical-source model ignores axial heat conduction based on the assumption that the axial temperature gradient is very small compared to the radial one. The analytical method is mathematically complex, and its solution could be time-consuming. To cope with this difficulty, an approximate algebraic solution has been introduced by Ramey, Chiu, and others; the list of the most important ones is provided in [23]. The infinite line source model comes with the assumption that the radial dimension of the well is significantly smaller than its axial length. The wellbore heat storage capacity is hence neglected. It is important to note that both models cannot handle the effect of ground surface and the accuracy of the results would be adversely affected for small operational timescales. Li and Lay [24] report, that the minimal elapsed operational time, τ , for use of any of these conventional models is $\tau > 5\tau_b$ as the thermal borehole approaches a steady-flux state. In this case, the temperature difference between the fluid and the wall of the borehole is constant. The associated time scale, τ_b , is defined by the following equation.

$$\tau_b = \frac{r_b^2}{a_b} \quad (11)$$

Ingersoll *et al.* [25] warn that the time ratio should be even higher to the minimize error associated with the infinite line source model, in particular $\tau > 20\tau_b$. A detailed discussion about these models is, however, beyond the scope of this paper. Instead, attention is paid to the derivation of the position of the far-field boundary condition, sometimes referred to as the radius of influence, r_{inf} . The radius of influence defines the interface between the zone within which the temperature is affected by the operation of the well and the zone beyond which remains undisturbed. Once determined, the boundary conditions can be fully described and applied for the calculation of the equivalent thermal resistance, see Section 4.3. It will be shown that the radius of influence can be derived directly from the infinite line-source model. The mathematical well heat transfer formulation of the problem approximated by the infinite line-source model is provided in the study of Li and Lai [24] and gives

$$\begin{aligned} \rho_g c_{p,g} \frac{\partial T_g}{\partial \tau} &= k_g \left(\frac{\partial^2 T_g}{\partial r^2} + \frac{1}{r} \frac{\partial T_g}{\partial r} \right) \\ r \rightarrow 0 & \quad -2\pi k_g \lim_{r \rightarrow 0} (r) \frac{\partial T_g}{\partial r} = q \\ r \rightarrow \infty & \quad T_g = T_{g,\infty} \\ \tau = 0 & \quad T_g = T_{g,\infty} \end{aligned} \quad (12)$$

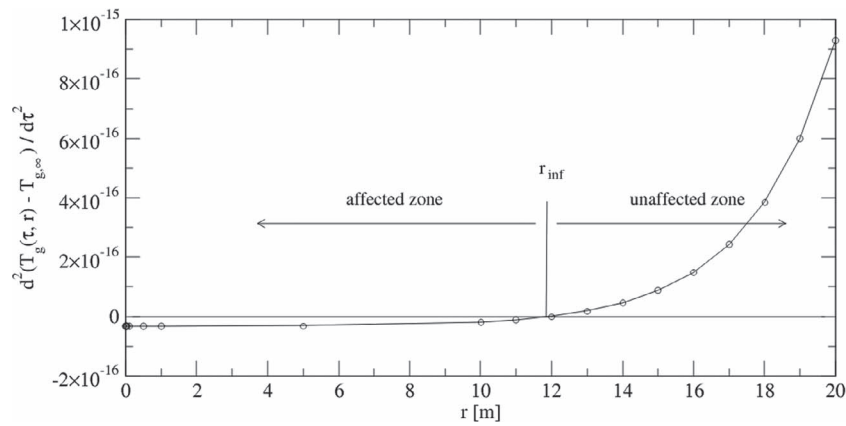


Figure 3. Behaviour of the second derivative of the g-function at 1 year of continuous operation.

where $T_g(\tau, r_b)$ is the ground temperature at time constant τ and radius of the borehole r_b and $T_{g,\infty}$ is the undisturbed temperature of the ground.

Ingersoll et al. [25] were the first who reformulate the problem using the so-called g-function $G(\tau, r)$, see Equation (13). The g-function refers to a parameter that characterizes the thermal response of the surrounding ground to a borehole heat exchanger. It is defined as the temperature response at a certain radial distance in the ground due to a unit of heat injected or extracted at the borehole wall, over a period of time and represents the solution to the transient heat conduction equation in cylindrical coordinates, accounting for the effects of thermal conduction and advection.

$$T_g(\tau, r) = T_{g,\infty} + q G(\tau, r) \quad (13)$$

For the infinite line-source model, the g-function can be expressed using the exponential integral, E_1 , see Equation (14) of a dummy variable u over the range of interest, i.e. from $r/4a\tau$ to infinity where $r = r_b$.

$$G(\tau, r) = \frac{1}{4\pi k_g} \int_{\frac{r^2}{4a_g\tau}}^{\infty} \frac{\exp(-u)}{u} du = \frac{1}{4\pi k_g} E_1\left(\frac{r^2}{4a_g\tau}\right) \quad (14)$$

In the context of heat conduction problems, the temperature distribution $G(\tau, r)$ represents how the temperature at a point r changes over time. The radius of influence, r_{inf} , specifies the interface between the affected and unaffected zone and hence it refers to a location in time where the rate of change of temperature with respect to time reaches a minimal value. Mathematically, this can be expressed using the second derivative of the g-function where $r = r_{inf}$ as follows:

$$\begin{aligned} & \frac{d^2(T_g(\tau, r) - T_{g,\infty})}{d\tau^2} \\ &= \frac{d^2(q G(\tau, r))}{d\tau^2} = q \frac{1}{4\pi k_g} \frac{e^{-\frac{r^2}{4a_g\tau}}}{\tau^2} \left(\frac{r^2}{4a_g\tau} - 1\right) = 0 \end{aligned} \quad (15)$$

The illustration of the behaviour second derivative of the g-function at 1 year of continuous operation for thermal diffusivity calculated according to the data in Table 5 is seen in Fig. 3.

Equation (15) is true when the last term $r^2/4a_g\tau - 1$ equals zero and hence the radius of influence can be calculated as a function of the thermal diffusivity of the wellbore formation and elapsed operational time as follows.

$$r_{inf} = 2\sqrt{a_g\tau} \quad (16)$$

The proposed expression is analogous to the derivation of the radius of investigation of the well [26] and was also used in the work of Alimonti and Soldo [6].

4 Description of the software

4.1 Software overview

WellTH is a brand-new tailor-made thermal-hydraulic simulation software written in C language dedicated to the assessment of the complex tasks related to the operation of the coaxial and multi-branch U-type DBHEs and capable of handling vertical, horizontal, and inclined wells. It comprises two basic modeling approaches—a quasi-steady-state assumption of the wellbore boundary based on the infinite line-source model being discussed in the previous section and a full transient approach based on a numerical discretization of the wellbore environment using the finite difference method discretization scheme. In addition to this, it can handle simulation of the drilling and through-tubing abandonment operation assuming a variation of the transfer line length over time and definition of the bottom hole lumped heat source for the modeling of the thermal disintegration processes within the wellbore as being the novel approach to the conventional drilling/milling techniques. For this paper, a brief description of the quasi-steady-state approach (using the r_{inf}) for the coaxial DBHE assessment is provided.

4.2 Flow parameters

The hydraulic diameter D_b , see Equation (17), is determined through a standard equation which gives the hydraulic diameter of the annulus the difference between the outer casing's inner diameter and the outer diameter of the central pipe.

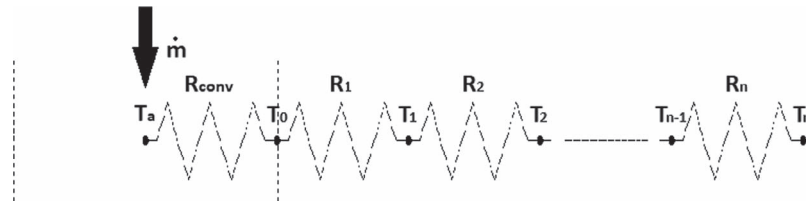


Figure 4. Multilayer heat structure substitution scheme representing wellbore environment.

Conversely, the hydraulic diameter of the upward-flow pipe corresponds directly to its internal diameter.

$$D_b = \frac{4 A_{\text{flow}}}{WP} \quad (17)$$

The calculation of the Darcy friction factor f depends upon the Reynolds number, Re . For laminar flow, the friction factor f_L follows a linear pattern, Equation (18). In the case of turbulent flow, the friction factor f_T is calculated using the implicit Colebrook–White formula [27] as shown in Equation (19). When encountering transitional flow, the friction factor f_P represents a Reynolds-weighted average of the laminar and turbulent values, see Equation (20). Note that a laminar flow regime in a conduit occurs when Re is less than 2000 while turbulent flow is established for Re higher than 4000. Transitional flow is assumed for Re values within this range.

$$f_L = \frac{64}{Re} \quad (18)$$

$$\frac{1}{\sqrt{f_T}} = -2 \log \left(\frac{SR}{3.7D_b} + \frac{2.51}{Re\sqrt{f_T}} \right) \quad (19)$$

$$f_P = f_T \frac{(Re - 2000)}{2000} + f_L \left[1 - \frac{(Re - 2000)}{2000} \right] \quad (20)$$

The Reynolds number is given by the following equation, where the characteristic length is the hydraulic diameter is D_b .

$$Re = \frac{\rho v L_{ch}}{\mu} \quad (21)$$

The annular flow channel is enclosed by two surfaces with possibly different roughness. Therefore, the average channel absolute roughness, SR , can be determined by calculating the perimeter-weighted average of these two values. Finally, the pressure drop in the flow elements is computed using Equation (22). The entry and exit losses, as well as the losses due to the pipe changes and turn at the bottom of the well, are disregarded.

$$\Delta p = \frac{1}{2} \rho \left(\frac{dl}{D_b} f \right) v^2 \quad (22)$$

The required pumping power P is determined using Equation (23). The density is computed for every element of the system, where subscript a stands for annulus and subscript c for the central pipe and η is the pump efficiency, taken in this

case as 0.85. The parameter n refers to the number of nodes in the discretization scheme.

$$P = \frac{1}{\eta} \sum_1^n \dot{m} \left[\left(\frac{\Delta p}{\rho} \right)_a + \left(\frac{\Delta p}{\rho} \right)_c \right] \quad (23)$$

4.3 Heat transfer in the wellbore vicinity

As mentioned above, the transient heat transfer in the wellbore environment is approximated using a quasi-steady state approach. The method is based on a calculation of the so-called equivalent thermal resistance of the heat structures. Since the wellbore structure may comprise several casings, the derivation of thermal resistance provided below aims at the generic equation for multilayer heat structure, as illustrated in Fig. 4. T_a is the temperature of the flow in the annulus and T_n is the temperature at r_{inf} , see Figs 2 and 4.

The Nusselt number, Nu , can be determined using various correlations found in the literature. The one proposed by Gnielinski [28] stands out as one of the most frequently used relationships.

$$Nu = \frac{\left(\frac{f}{8} \right) (Re - 1000) Pr}{1 + 12.7 \sqrt{\left(\frac{f}{8} \right)} \left(\sqrt[3]{Pr^2 - 1} \right)} \quad (24)$$

In our simulations, the Re number ranged from laminar values at the low volumetric flow rates up to 8.5 lpm in the central pipe and 30 lpm in the annular conduit. The turbulent flow regime starts at 17 lpm in the central pipe and 60 lpm in the annular conduit, respectively. It needs to be clarified, that these values are just approximate, the real values are temperature and hence case dependent. The proposed Gnielinski equation is valid within a range of $3000 < Re < 5 \cdot 10^6$ and $0.5 < Pr < 2000$. For the laminar flow ($Re < 2000$), a mixed surface boundary condition can be assumed (i.e. the surface is not at constant heat or constant temperature). For this case, a conservative value of $Nu = 3.66$ [13] was used. Since there is no dedicated correlation for the transitional regime ($2000 < Re < 3000$), the laminar conditions were applied. The possible simplifications in the laminar and transitional regimes are not critical as this forms only a small part of the range studied and does not affect conclusions that have been reached.

The heat transfer coefficient, h , is calculated using the following equation, where the characteristic length, L_{ch} , equals the hydraulic diameter, D_b , for both circular and annular channels.

$$h = \frac{Nu k_f}{L_{ch}} \quad (25)$$

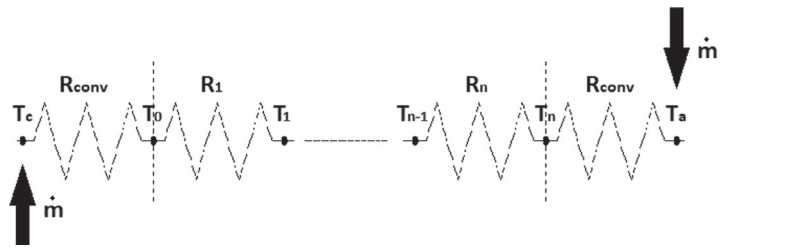


Figure 5. Multilayer heat structure substitution scheme representing central pipe.

Subsequently, the thermal resistance of the external multilayer heat structure R_{ext} can be determined for a given time from the start of the operation as shown in Equation (26). The subscript i refers to the different layers whereas n denotes the number of radial layers. The outer radius of the outermost layer equals the radius of influence (16), so that, $r_n = r_{inf}$.

$$R_{ext} = \frac{1}{h_a A_{a,out}} + \sum_{i=1}^n \frac{\ln\left(\frac{r_i}{r_{i-1}}\right)}{2 \pi dl k_i} \quad (26)$$

where $A_{a,out}$ is the heat transfer area at the outer surface of the annular conduit.

The rate of heat flow for the external heat structure \dot{Q}_{ext} can be computed using the following equation, where the far-field temperature of the rock formation is calculated as a function of surface temperature, temperature gradient, and depth, see Section 5.

$$\dot{Q}_{ext} = \frac{\Delta T}{R_{ext}} = \frac{T_\infty - T_a}{R_{ext}} \quad (27)$$

4.4 Heat transfer in the central pipe

The simulation of the heat transfer through the central pipe can be done using the steady-state heat transfer equation. Also, in this case, the derivation of the thermal resistance R_{int} for the multilayer heat structure is given in Fig. 5. For homogeneous pipe, simply assume $n = 1$. T_c is the temperature of the water flowing up the central pipe, see Fig. 2.

$$R_{int} = \frac{1}{h_c A_c} + \sum_{i=1}^n \frac{\ln\left(\frac{r_i}{r_{i-1}}\right)}{2 \pi dl k_i} + \frac{1}{h_a A_{a,in}} \quad (28)$$

The second term in Equation (28) is the summation of the resistances of the steel pipes and the insulation. The coefficient, h_c , is the heat transfer coefficient at the circular conduit calculated using Equations (24) and (25) above. The heat transfer coefficient, denoted as h_a , is numerically identical at both the inner and outer surfaces of the annular conduit. The rate of heat flow for the heat structure, \dot{Q}_{int} , can be calculated similar to \dot{Q}_{ext} as follows.

$$\dot{Q}_{int} = \frac{\Delta T}{R_{int}} = \frac{T_c - T_a}{R_{int}} \quad (29)$$

Assessment of the contribution of radiative heat transfer within the central pipe (VIT) to the overall thermal resistance

makes the calculation more challenging, see Fig. 6. To streamline the derivation process, let's assume three-layer geometry. The first and the third layers consist of solid material where only the thermal conduction heat transfer process is assumed. The second layer contains an air gap where both thermal conduction and radiation are considered.

The thermal resistance of the heat structure is then described using (30) and the rate of heat flow for the external heat structure \dot{Q}_{int} can be calculated according to the Equation (29) provided above. The solution of Equations (29) and (30) can be found using one of the root-finding methods, such as the bisection method which is implemented in WellTH software.

$$R_{int} = \frac{1}{h_c A_c} + \frac{\ln\left(\frac{r_1}{r_0}\right)}{2 \pi dl k_1} + \frac{1}{\frac{1}{\frac{1}{\ln\left(\frac{r_2}{r_1}\right)} + \frac{1}{h_{rad} A_1}} + \frac{\ln\left(\frac{r_3}{r_2}\right)}{2 \pi dl k_3} + \frac{1}{h_a A_{a,in}}} \quad (30)$$

4.5 Coupling between the heat structure models and flow zones

Description of the interface between the heat structures and flow zones is a necessary part of the calculation routine. Such is described using a simple calorimetric equation yielding the change of temperature in corresponding elements of the cylindrical ΔT_c and annular ΔT_a conduits, respectively.

$$\Delta T_c = \frac{\dot{Q}_{int}}{\dot{m} * c_p} \quad (31)$$

$$\Delta T_a = \frac{\dot{Q}_{ext} - \dot{Q}_{int}}{\dot{m} * c_p} \quad (32)$$

4.6 Software validation

Unfortunately, there is only a limited pool of published experimental data containing the requisite information to allow the validation of the simulation process. Furthermore, the operation of existing geothermal installations is affected by seasonal demands and intermittently interrupted by maintenance, thereby complicating comparisons. Moreover, descriptions of real geothermal systems are often precarious, with factors such as rock porosity, underground water flows, cracks in cement behind casing structures, uncertain lithostratigraphy,

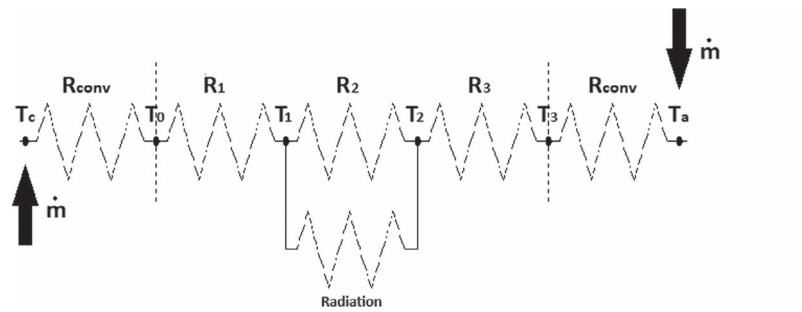


Figure 6. Three-layer heat structure substitution scheme representing central rod assuming radiative heat transfer.

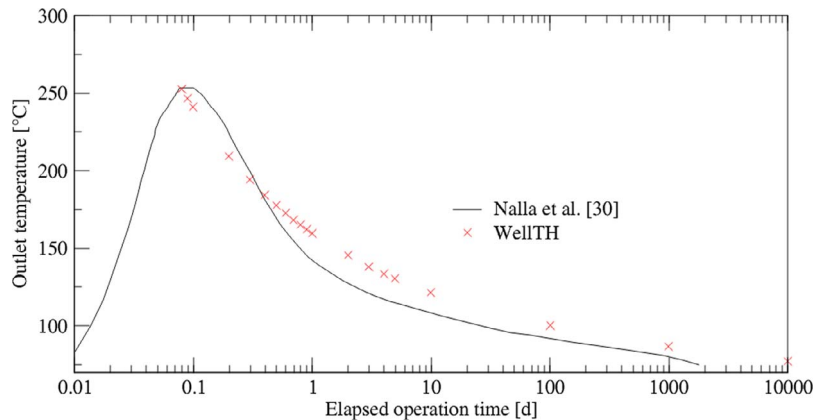


Figure 7. Temperature of the fluid at the outlet of the well, adapted from Nalla *et al.* [29].

and material properties’ dependency on temperature potentially undermining the accuracy of any attempted comparisons. Given these circumstances, it was concluded that validation among different codes could be sufficient, at least for now. The simulation software underwent validation against the study [29], with the results illustrated in Fig. 7.

The minor discrepancy in comparison of the results can be primarily attributed to the selected simulation approach. As discussed in Section 3, the infinite line-source model is not applicable for short-term analysis. Secondly, the simulation model used in the study of reference [29] disregards the transport properties of the fluid and does not assume friction losses in the system. Thirdly, the results provided in the referenced document were presented in a graphical form and had to be extracted manually for the above comparison. The comparison however is very good in verifying the reliability of the solution methodology outlined above.

5 Simulation

As mentioned above, the assessment of the VIT requires detailed design specifications and a comprehensive 3D simulation tool. The goal of this study is, however, to assess the impact of air gap pressure and surface emissivity on the DBHE thermal response; hence, only a simplified VIT design made of two concentric tubular units was studied here. The 1D approach is fairly applicable for such an analysis and will yield reasonable results. In addition, the study provides data related to the variation in DBHE length, operational timescale considerations, and optimization of the mass flow rate for the highest possible temperature output at the wellhead.

The wellbore geometry contains a casing structure of outer diameter 198.52 mm with a thickness of 10.36 mm of uniform

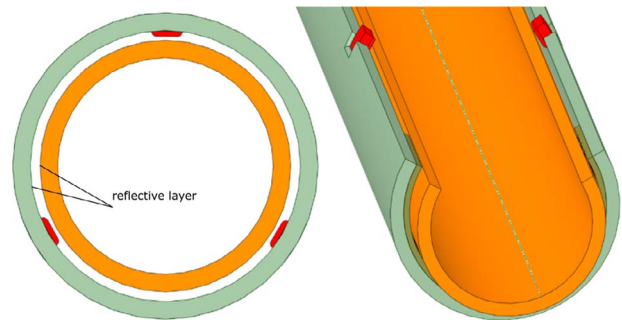


Figure 8. Design of the VIT.

Table 6. Boundary conditions.

Elapsed operational time	1 year
Inlet volumetric flow rate	100 lpm
Inlet fluid temperature	10 °C
Surface temperature	15 °C
Geothermal gradient	30°C/km

dimensions throughout the entire length of the well. These dimensions are not directly related to API SPEC 5CT [30], but the software allows all given dimensions in this reference to be tested easily in a future study. Although the WellTH can handle wells in inclination, only the straight vertical geometry is considered for now. The gap between the casing and the 215.9 mm (8 1/2 “) borehole is cemented with a thin layer of material. The resistance of this thin layer of cement is included in the calculations. It is only ignored when calculating the radius of influence. Two types of central pipe geometry have

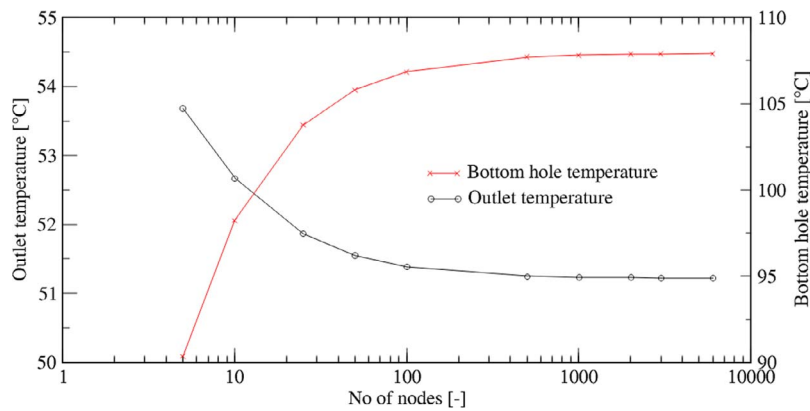


Figure 9. Effect of axial nodalization on fluid temperature (depth is 6 km).

been selected for this study—a homogeneous pipe made of HDPE material and VIT that consists of two coaxial steel tubings separated by the gap filled with air at various pressure levels. The outline of the DBHE geometry and indication of the axial nodalization of the computational domain is depicted in Fig. 2. The inner and outer diameters of the central pipe are the same for both HDPE and VIT systems. The design of the VIT is provided in Fig. 8. The reflective layer is assumed at both internal surfaces of the gap layer and the clearance between both steel tubings is preserved using a set of pins. The parasitic heat conductivity through the pins is neglected. For the outer shell, a 139.7 mm (5.5”) casing with a 10.54 mm thickness was chosen, while for the inner shell, a 101.6 mm (4”) tubing with a 6.65 mm thickness (per API SPEC 5CT) was opted for, resulting in an 8.51 mm clearance for vacuum insulation.

The list of applicable boundary conditions is shown in Table 6 below. The provided boundary conditions are valid for each analyzed case with few exceptions, which are identified at the point of reference.

A wellbore static far-field ground temperature $T_{g,\infty}$ is defined using the Dirichlet boundary condition at r_{inf} for each axial layer as follows:

$$T_{g,\infty} = T_{surf} + L G_{grad} \quad (33)$$

where L is the axial distance of the node centre from the surface.

The effect of axial nodalization has been investigated using the homogeneous HDPE central pipe. Employing a coarse nodalization across the computational domain will lead to inaccurate outcomes. Conversely, employing an overly detailed nodalization might provide good results, albeit at the expense of a simulation time. For this study, a 6-km long wellbore is studied as this provides a more detailed resolution of temperature response behaviour. Although the obtained results depicted in Fig. 9 indicate fluid temperature stabilization for a resolution of one node per six meters of DBHE length, a conservative setup of two nodes per meter is used in subsequent simulations for improved accuracy.

5.1 Assessment of reference scenarios

The following set of simulations was done for a length of 3 km. The WellTH simulation software, at this point, does not allow for the specification of material properties of solids with respect to temperature. Based on the boundary condition

Table 7. k -value of the VIT pipe at 40°C

Pressure [Pa]	$k(p)/k_0$ [-]	k -value [W/mK]
1.0E-02	0.003	0.00024
1.0E-01	0.033	0.00267
1.0E+00	0.257	0.02081
1.0E+01	0.769	0.06224
1.0E+02	0.971	0.07857
1.0E+03	0.997	0.08067
1.0E+04	1.000	0.08091
1.0E+05	1.000	0.08091

of Table 6, the static bottom hole temperature would be 105°C, therefore an average pipe temperature to be 40°C can be assumed. The thermal conductivity of air at 40°C and standard atmospheric pressure yields 0.02735 W/mK [19] and is significantly lower than the conductivity of steel. For the given geometry and if no radiative heat transfer is considered, the equivalent 1D thermal conductivity of the VIT pipe (k -value) can be calculated using Equation (34) and equals 0.0809 W/mK.

$$k\text{-value} = \frac{\ln \frac{r_3}{r_0}}{\sum_{i=1}^3 \frac{\ln \left(\frac{r_i}{r_{i-1}} \right)}{k_i}} \quad (34)$$

The air gap makes the highest contribution to the overall thermal resistance and affects the thermal response of the system the most. The steel properties have only minor effects. For instance, if the pipe shells were manufactured from austenitic steel with a thermal conductivity of 15 W/mK instead of the original carbon steel with a conductivity of 45 W/mK, the k -value would drop to 0.0807 W/mK, i.e. makes only 0.24% difference. As discussed in Section 2.2, the conductivity of the gap and hence k -value of the pipe can be greatly impacted by the gas pressure. If the absolute pressure of 10 Pa is maintained within the VIT annulus, the k -value drops to 0.0622 W/mK making a 23.1% reduction compared to the reference value. The effect of gas pressure on the k -value of the VIT pipe is provided in Table 7.

It has been already discussed that the VIT design generally includes an internal refractive layer to minimize radiative heat transfer. The simulation matrix for these conditions, given in Tables 8 and 9, also contains cases where the refractive

Table 8. Outlet temperature [°C] of DBHE with VIT for 3 km

	Pressure [Pa] <i>k</i> -value [W/m.K]	1.0E-02	1.0E-01	1.0E+00	1.0E+01	1.0E+02	1.0E+03	1.0E+04
		0.00024	0.00267	0.02081	0.06224	0.07857	0.08067	0.08091
Surface emissivity [–]	0.03	54.6	54.4	52.8	49.6	48.5	48.4	48.4
	0.95	44.7	44.6	43.6	41.6	40.9	40.8	40.8

Table 9. Thermal output [kW] of DBHE with VIT for 3 km

	Pressure [Pa] <i>k</i> -value [W/mK]	1.0E-02	1.0E-01	1.0E+00	1.0E+01	1.0E+02	1.0E+03	1.0E+04
		0.00024	0.00267	0.02081	0.06224	0.07857	0.08067	0.08091
Surface emissivity [–]	0.03	309.6	308.0	297.2	275.2	267.3	266.4	266.3
	0.95	240.7	239.8	233.2	219.5	214.5	213.9	213.8

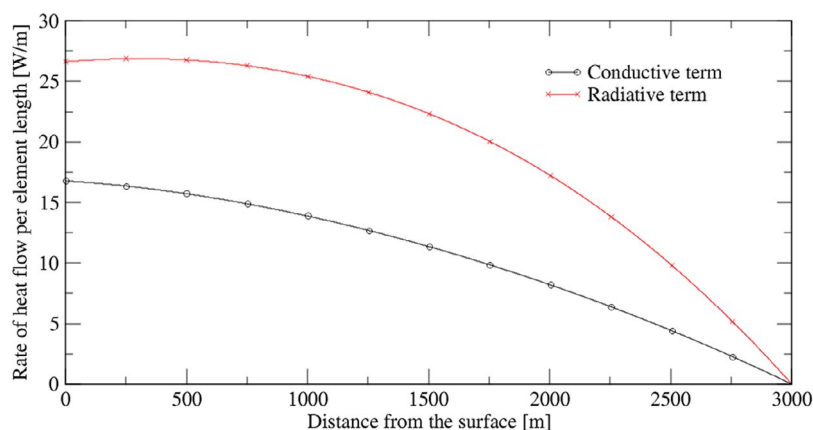


Figure 10. Rate of heat flow through VIT per element length (0.5 m).

material is not used to evaluate the effect of radiative heat transfer on the overall response of the system. It should be noted that the *k*-value of the VIT pipe is, under any pressure conditions, significantly lower than the thermal conductivity of the HDPE pipe, which equals 0.54 W/m.K. The DBHE system with HDPE produces a fluid outlet temperature of 31.6°C and a thermal output of 149.7 kW, which is way lower than DBHE with VIT.

The simulation data indicate that an annular VIT pressure level of 10 Pa does not significantly affect the thermal response of the DBHE system compared to the pipe with an annular pressure close to the normal atmospheric one. A better thermal result can be obtained after pressure reduction to 1 Pa, or even to 0.1 Pa. A further pressure reduction below 0.1 Pa appears not to be of any benefit. It should be also noted at this stage that there is no information if such low pressures can be maintained in the VIT system. In all cases, the use of the VIT system yields much better results than the HDPE pipe as the presence of an air gap at any pressure provides much better thermal insulation than the homogeneous polymer. On the other hand, gap pressure close to the atmosphere may promote weak natural convection, which would intensify heat transfer, as per Section 2.3. The effect of surface emissivity is more important than the effect of the gap pressure. Figure 10 shows the rate of heat flow through the air gap per element length with respect to the distance of the element from the surface. The length of the element is given by nodalization and yields 0.5 m. In this case, the most conservative scenario was selected, i.e. surface emissivity equals 0.95 and annular

pressure is 10⁴ Pa. The heat is transferred via conduction and radiation in parallel and it is obvious that nearly twice as much heat is transferred through the radiative term. Note that if we use an emissivity of 0.03 the radiative term is very small, i.e. 0.6 W/0.5 m elemental length.

Based on the above it can be concluded that the presence of a low-pressure environment in the VIT annulus at the level of 10 Pa and higher has nearly no effect on the DBHE response. On the other hand, the maintenance of low pressure is important to prevent hydrogen build-up during the hydrogen permeation process with consequences that would lead to a significant increase in the pipe's *k*-value. The radiative term has a higher impact on the heat transfer through the VIT pipe than the conductive term and can be minimized by VIT design using reflective layers. In all cases, the VIT performance significantly outperforms the HDPE pipe for the DBHE applications.

5.2 Variation with elapsed operational time

Section 3 demonstrates that thermal resistance of the wellbore environment is contingent upon the duration of operation of the DBHE system. As time progresses, the radius of influence r_{inf} (16) expands subsequently elevating the thermal resistance. This implies a reduced rate of heat flow through the external boundary of the system $Q_{i,ext}$ over time. Figure 11 shows a comparison of DBHE outlet temperatures for a 3 km long system. Two systems have been analysed—a DBHE system with a central pipe made of HDPE material and the DBHE containing the VIT pipe with an annular pressure of

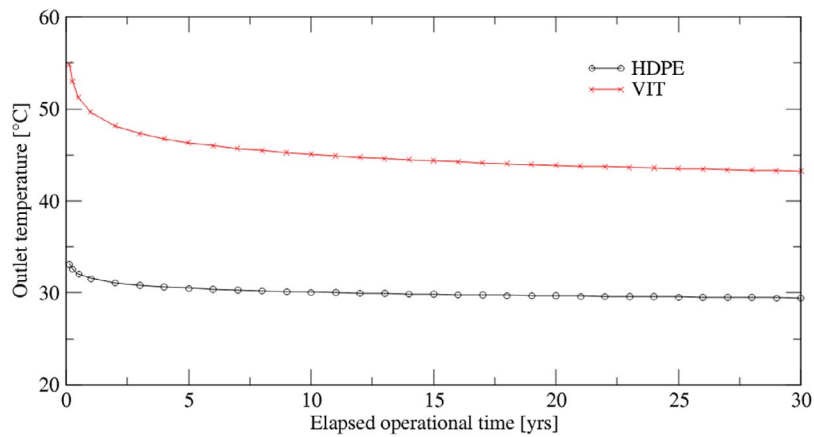


Figure 11. DBHE outlet temperature as a function of operational time (3 km).

Table 10. Outlet temperature [°C] for DBHE—1 km well with VIT

		1.0E-02	1.0E-01	1.0E+00	1.0E+01	1.0E+02	1.0E+03	1.0E+04
Pressure [Pa]		1.0E-02	1.0E-01	1.0E+00	1.0E+01	1.0E+02	1.0E+03	1.0E+04
<i>k</i> -value [W/m.K]		0.00024	0.00267	0.02081	0.06224	0.07857	0.08067	0.08091
Surface emissivity [–]	0.03	17.8	17.8	17.7	17.6	17.6	17.6	17.6
	0.95	17.5	17.5	17.5	17.4	17.4	17.4	17.4

Table 11. Thermal output [kW] for DBHE—1 km well with VIT.

		1.0E-02	1.0E-01	1.0E+00	1.0E+01	1.0E+02	1.0E+03	1.0E+04
Pressure [Pa]		1.0E-02	1.0E-01	1.0E+00	1.0E+01	1.0E+02	1.0E+03	1.0E+04
<i>k</i> -value [W/m.K]		0.00024	0.00267	0.02081	0.06224	0.07857	0.08067	0.08091
Surface emissivity [–]	0.03	53.9	53.8	53.5	52.8	52.6	52.6	52.6
	0.95	52.1	52.1	51.8	51.2	51.0	51.0	51.0

Table 12. Outlet temperature [°C] for DBHE—5 km well with VIT.

		1.0E-02	1.0E-01	1.0E+00	1.0E+01	1.0E+02	1.0E+03	1.0E+04
Pressure [Pa]		1.0E-02	1.0E-01	1.0E+00	1.0E+01	1.0E+02	1.0E+03	1.0E+04
<i>k</i> -value [W/m.K]		0.00024	0.00267	0.02081	0.06224	0.07857	0.08067	0.08091
Surface emissivity [–]	0.03	104.0	103.1	96.5	84.4	80.5	80.0	79.9
	0.95	62.8	62.5	60.3	55.9	54.4	54.2	54.2

10 Pa and surface emissivity of 0.03. Note that a VIT system with such a setup will be hereinafter in this document referred to as the *realistic VIT case*.

5.3 Variation with DBHE length

The following section covers the effect of DBHE length on the thermal output of the system, examining 1 km and 5 km long heat exchangers. Data related to DBHE operated with the VIT system are provided in Tables 10 and 11 for the 1 km and Tables 12 and 13 for the 5 km case, respectively. For the 1 km case, the DBHE system with HDPE central pipe provides a fluid outlet temperature of 16.7°C and a thermal output of 46.7 kW. Comparing the thermal output gains, the HDPE case provides roughly 88% of the realistic VIT case. The difference here is less pronounced compared to the nearly 50% observed in the 3 km cases included in Table 9. In addition to this, no remarkable difference is observed for either VIT annular pressure or surface emissivity dependency. Such a system response can be explained by the much shorter length, i.e. smaller heat transfer area of the pipe

and low ambient temperatures, which minimize the radiative heat transfer term.

The situation significantly changes for the 5 km long DBHE system. The system with HDPE pipe can only deliver 37.9°C at the wellhead outlet and 193.5 kW of thermal output, which is only 37% of the power delivered by the realistic VIT case, see Tables 12 and 13. For this depth, the surface emissivity of the internal VIT structures has a decisive impact on the thermal response of the system due to the increased heat transfer area and much higher ambient temperatures. The annular pressure effect exhibits some outlet temperature improvement at 10 Pa but similarly to the 3 km case, the absolute pressure reduction to 0.1–1 Pa would be of greater benefit. Further pressure decrease below 0.1 Pa has no substantial impact.

The analysis performed has shown that there is only a limited technical reason for the usage of VIT pipes in shallow DBHE systems and the key VIT parameters, such as annular pressure and surface emissivity have only negligible impact on the DBHE response. The importance of VIT pipe increases

Table 13. Thermal output [kW] for DBHE—5 km well with VIT.

Pressure [Pa]		1.0E-02	1.0E-01	1.0E+00	1.0E+01	1.0E+02	1.0E+03	1.0E+04
k -value [W/m.K]		0.00024	0.00267	0.02081	0.06224	0.07857	0.08067	0.08091
Surface emissivity [–]	0.03	655.0	648.3	602.2	517.4	490.0	486.6	486.3
	0.95	366.9	364.7	349.5	319.0	308.4	307.0	306.9

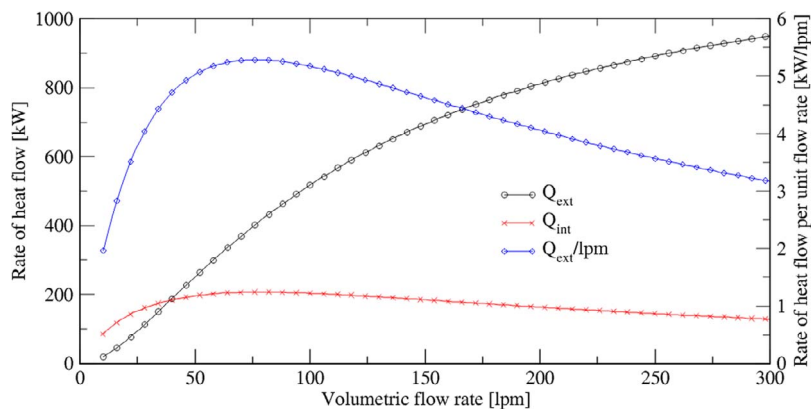


Figure 12. Heat transfer rate through the heat structures (VIT and 5 km depth).

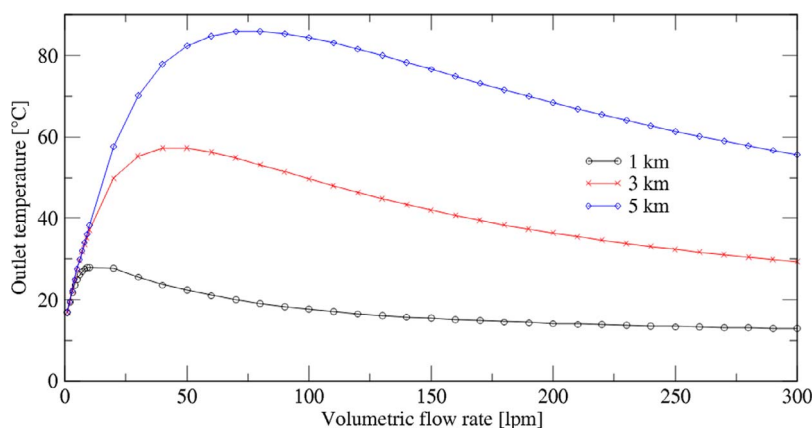


Figure 13. DBHE outlet temperature as a function of flow rate for various lengths of the system (VIT).

with the length of the system where the thermal response tends to be significantly improved over to HDPE pipes.

5.4 Optimization of the mass flow rate

In certain applications, such as electricity generation, it might be necessary to maximize outlet temperature from the DBHE to achieve the highest possible enthalpy of the fluid. For a given geometry of the system, this can be done relatively easily by changing the inlet flow rate of the fluid. The outlet fluid temperature tends to rise at low flow rates reaching its maximal value at a certain point and then subsequently decreasing with further volumetric flow increase. However, such an optimization always happens at the expense of the thermal output produced by the wellbore. The behaviour of the DBHE system will be further explained using the realistic VIT case with a system length of 5 km. Figure 12 shows the overall rate of heat flow through the external wellbore boundary Q_{ext}^i and through the VIT pipe Q_{int}^i . The heat transfer through the external boundary increases sharply with the flow rate at the beginning as the nature of the flow changes from laminar to turbulent. Subsequently, the increase becomes

flatter, and it is driven by the continuous increase of the velocity which positively affects the heat transfer coefficient as well as by the decrease of the fluid temperature in the annular conduit. Beyond the point of optimal flow rate, the effect of increasing flow rate outbalances the change of Q_{ext}^i , the heat transfer rate per unit flow rate Q_{ext}^i/lpm starts to decrease hence causing a decrease in the DBHE outlet temperature, see Fig. 13. Conclusively, it can be written that the maximal temperature is always achieved for the maximal Q_{ext}^i/lpm ratio. The rate of heat flow through the VIT pipe Q_{int}^i is driven by temperature difference between the fluid channels and affected by the flow parameters as well. For small flow rates heat is being transferred from the cylindrical to the annular conduit and Q_{int}^i exceeds Q_{ext}^i . Note however, that there is no heat transfer imbalance, i.e. the heat transfers are within the system. The reason for the initially higher Q_{int}^i lies in higher temperature gradient between adjacent flow zones and higher Re in the cylindrical inner tube for this specific geometry. Conversely, a further decrease of Q_{int}^i is dominantly caused by reduced temperature gradient with increasing flow rate. Also, Q_{int}^i reaches maximal value at the point of optimal

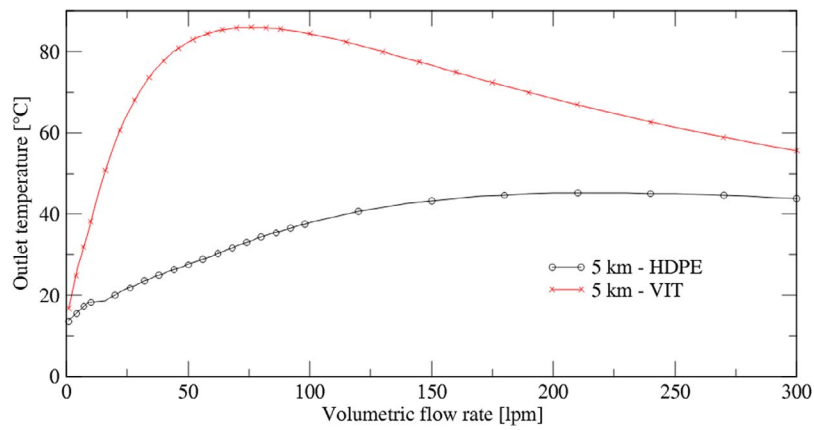


Figure 14. DBHE outlet temperature as a function of flow rate—5 km, HDPE vs VIT.

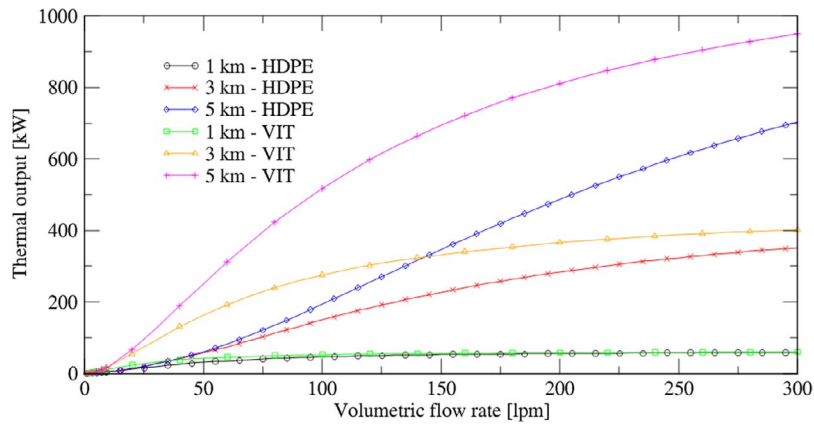


Figure 15. DBHE thermal output as a function of flow rate for various lengths of the system.

flow rate due to the highest temperature gradient between the flow zones.

Simulation results provided in Fig. 13 indicate a significant impact of the DBHE length on the optimal flow rate. The reasoning for this is straightforward; the shorter the DBHE system, the smaller the heat transfer through the external wellbore boundary $Q_{i_{ext}}$. Since the maximal outlet temperature is always achieved for the maximal heat transfer rate per unit flow rate $Q_{i_{ext}}/lpm$, the optimal flow rate is smaller for shorter systems.

The optimal flow rate for the maximal temperature outlet also significantly depends on the central pipe configuration. For a central pipe configuration with a higher k -value (HDPE), the optimal flow rate point is shifted towards higher values, see Fig. 14.

The effect of the volumetric flow rate on the thermal output for three different DBHE depths is depicted in Fig. 15. As seen in the figure, the depth has a very significant effect with the thermal output beginning to demonstrate a plateau at about 300 lpm (approximately 5 kg/s) for short systems. The substantial effect of the better thermal insulation properties of the VIT system is obvious for depths greater than 1 km, for the conditions examined in this paper.

The previous work of the present authors [31] has shown that lower insulation properties of the central rod led to higher bottom hole temperatures and elevated fluid temperature in the annular zone. This is caused by the increased rate of heat flow from the cylindrical to the annular conduit. Consequently, the rate of heat flow through the external boundary

$Q_{i_{ext}}$ for the HDPE pipe is lower compared to the realistic VIT case due to a smaller temperature gradient between the wellbore wall and annular fluid, see Fig. 16. The heat transfer rate per unit flow rate $Q_{i_{ext}}/lpm$ is directly linked to the outlet temperature via a calorimetric equation and hence it is also the reason why the temperature outlet from the well is lower for systems with higher k -values. This shift in optimal flow rate between VIT and HDPE pipe occurs because the increased efficiency of heat transfer through the central pipe allows for faster heat exchange, requiring a higher flow rate to maintain equilibrium between the fluid temperature and the ground temperature. In other words, the lower possible bulk fluid temperature in the annular zone can be found by employing an optimal flow rate thus reaching the maximal $Q_{i_{ext}}/lpm$ ratio for a given geometry.

5.5 Estimation of pumping power

Figure 17 shows the pumping power, see (23), required to maintain the desired volumetric flow rate through the DBHE system. The efficiency of the pump in these calculations was taken as 0.85. The power required is only a fraction of the thermal power output and this could be considered in the design and operation of geothermal systems. For the realistic VIT case, the pumping power represents only $\sim 2.2\%$ (1 km case), $\sim 1.2\%$ (3 km case), and $\sim 1.0\%$ (5 km case) of the thermal outlet from the DBHE system. The data above were obtained for one year of continuous operation. However, it is worth noting that pumping power will not significantly

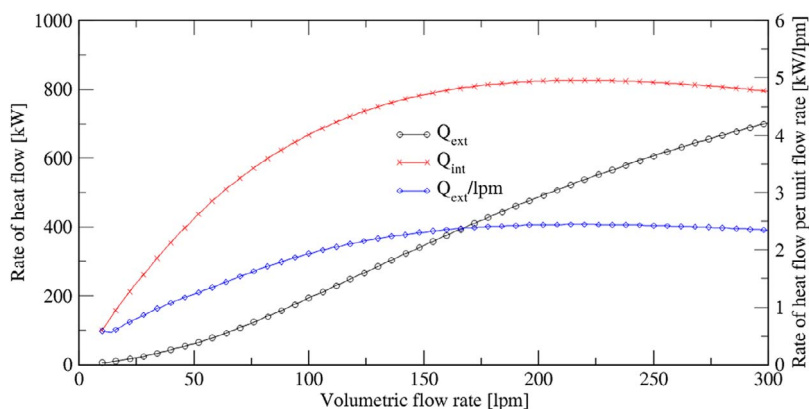


Figure 16. Heat transfer rate through the heat structures—HDPE and 5 km.

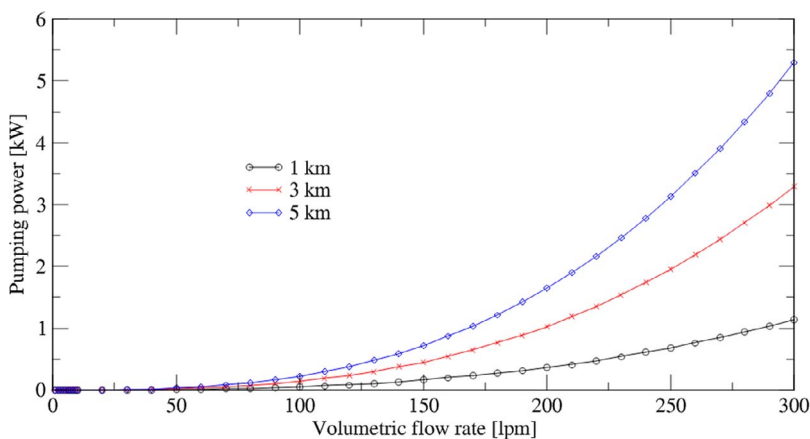


Figure 17. Pumping power as a function of flow rate for various lengths of the system (VIT).

change with elapsed operational time as the temperature dependence of water material properties can be neglected within the expected range.

6 Conclusions

This paper aims to evaluate the performance of the gap-insulated central pipe for DBHE applications and delivers a comparison with the homogeneous HDPE pipe. It examines the impact of varying air-gap pressure levels together with the central pipe surface emissivity on the DBHE's thermal response. The effect of the air gap pressure on the pipe's thermal conductivity and the possibility of free convection within the pipe were theoretically assessed. The paper provides a derivation of the radius of influence of the well based on the infinite line-source model. It has been found that the vacuum level in the standard VIT pipes (~ 10 Pa) seems inadequate in reducing the thermal conductivity of the low-pressure gas layer. Furthermore, it can be inferred that the presence of a low-pressure environment prevents natural convection in the air gap.

The simulation part has been conducted using the WellTH simulation software. First, the requirements for the axial nodalization of the computational domain have been discussed. Subsequent work was focused on a comparison of the HDPE and VIT central pipe systems for reference DBHE length of 3 km. It has been found that the VIT pipe system outperforms significantly the HDPE pipe at any internal pressure conditions regardless of the use of a reflective layer, see

for example Fig. 15. Simulation data indicate that an annular VIT pressure level of 10 Pa does not significantly affect the thermal response of the DBHE system compared to the pipe with annular pressure close to the normal atmospheric one. Thermal yields can be significantly improved with VIT annular pressure at a level of 0.1–1 Pa. A further pressure reduction below 0.1 Pa brings no additional benefit. The radiative term exerts a greater influence on the heat transfer through the VIT pipe than the conductive term and can be reduced by VIT design using reflective layers.

It has also been found that the advantage of employing the VIT system diminishes in shallow DBHE systems, less than 1 km deep, where the simple homogeneous HDPE pipes can deliver comparable results at more approachable costs. In that case, the thermal output provided by the system using HDPE pipe provided $\sim 88\%$ of the realistic VIT case. However, the use of VIT would yield superior outcomes for deeper wells, particularly considering the strict temperature limitations of HDPE pipes. Data obtained for a 5 km long system showed that the DBHE system with an HDPE pipe can produce only 37% of the thermal power delivered by the realistic VIT case. A further study focused on flow rate optimization revealed that the relationship between the maximal outlet temperature and flow rate varies depending on the DBHE configuration, including factors like wellbore length and insulation properties of the central pipe. Such an optimization should be tailored to each individual DBHE design and should not be difficult to perform with appropriate software.

It has also been found that the required pumping power represents only a small fraction of the total thermal outlet from the DBHE system if the VIT tubing is used. The pumping power required was also predicted and was found to be a fraction of the thermal output, i.e. $\sim 2.2\%$, $\sim 1.2\%$, and $\sim 1.0\%$ for the 1, 3, and 5 km wells with VIT respectively.

Author contributions

Ján Kubačka (Conceptualization [equal], Data curation [equal], Formal analysis [equal], Funding acquisition [supporting], Investigation [equal], Methodology [equal], Resources [equal], Software [lead], Supervision [supporting], Validation [equal], Visualization [equal], Writing—original draft [lead], Writing—review and editing [equal]) and Tassos Karayiannis (Conceptualization [equal], Formal analysis [equal], Funding acquisition [lead], Investigation [equal], Methodology [equal], Project administration [equal], Resources [lead], Software [supporting], Supervision [lead], Validation [equal], Writing—original draft [Supporting], Writing—review and editing [equal]).

Funding

None declared.

REFERENCES

- Kolo I, Brown CS, Falcone G. Thermal power from a notional 6 km deep borehole heat exchanger in Glasgow. In: *Proceedings of the 48th Workshop on Geothermal Reservoir Engineering*, 6th–8th February 2023, Stanford, CA. Stanford University; 2023, 1–10
- Barbier E. Geothermal energy technology and current status: an overview. *Renew Sust Energy Rev* 2002;6:3–65. [https://doi.org/10.1016/S1364-0321\(02\)00002-3](https://doi.org/10.1016/S1364-0321(02)00002-3).
- Bu X, Ma W, Li H. Geothermal energy production utilizing abandoned oil and gas wells. *Renew Energy* 2012;41:80–5. <https://doi.org/10.1016/j.renene.2011.10.009>.
- Templeton JD, Ghoreish-Madiseh SA, Hassani F. *et al.* Abandoned petroleum Wells as sustainable sources of geothermal energy. *Energy* 2014;70:366–73. <https://doi.org/10.1016/j.energy.2014.04.006>.
- Wang K, Yuan B, Ji G. *et al.* A comprehensive review of geothermal energy extraction and utilization in oilfield. *J Pet Sci Eng* 2018;168:465–77. <https://doi.org/10.1016/j.petrol.2018.05.012>.
- Alimonti C, Soldo E. Study of geothermal power generation from a very deep oil well with a wellbore heat exchanger. *Renew Energy* 2015;86:292–301. <https://doi.org/10.1016/j.renene.2015.08.031>.
- Śliwa T, Kruszewski M, Zare A. *et al.* Potential application of vacuum insulated tubing for deep borehole heat exchangers. *Geothermics* 2018;75:58–67. <https://doi.org/10.1016/j.geothermics.2018.04.001>.
- PetroPi Industries. *Vacuum Insulation Tubing (VIT)*. <http://www.petropi.com/vacuum-insulation-tubing.html> (12 March 2024, date last accessed).
- Cormier K. Effective design of insulated tubing for a sour environment. *SPE Prod Eng* 1990;5:221–4. <https://doi.org/10.2118/17103-PA>.
- TMK-Group. *Vacuum Insulation Tubing*. <https://www.tmk-group.com/VIT> (12 March 2024, date last accessed).
- Azzola J, Pattilo P, Richey JF. *et al.* 2004. The heat transfer characteristics of vacuum insulated tubing. In *SPE Annual Technical Conference and Exhibition, 26th - 29th September 2004*. Houston, TX, USA: Society of Petroleum Engineers. 1–8.
- Zhou C, Zhu G, Xu Y. *et al.* Novel methods by using non-vacuum insulated tubing to extend the lifetime of the tubing. *Front Energy* 2015;9:142–7. <https://doi.org/10.1007/s11708-015-0357-7>.
- Incropera FP, Dewitt DP, Bergman TL. *et al.* *Principles of Heat and Mass Transfer*. 7th ed. Hoboken, NJ: John Wiley & Sons, 2017.
- Schaa SA, Chambre PL. *Flow of rarefied Gases*. Princeton, NJ: Princeton University Press, 1961.
- Ismail AF, Khulbe KC, Matsuura T. *Gas Separation Membranes: Polymeric and Inorganic*. Heidelberg: Springer Cham, 2015.
- Tome AE. 1982. Fluid Flow Volume. Section 410.2. In Manglik R, White FM (eds). *Heat Transfer Data Book*. Amsterdam, New York, USA: Genium Publishing Corporation. 8.
- Geiser DR, Goldthwaite WH. Experimental determination of the viscosity of air in the gaseous state at low temperatures and pressures. Battelle Memorial Institute. Report number: AEDC-TDR-63-143. 1963.
- Pippard AB. *Elements of Classical Thermodynamics*. London: The Syndics of the Cambridge University Press, 1966.
- The National Institute of Standards and Technology. *NIST Chemistry WebBook*. <https://webbook.nist.gov/chemistry/> (Accessed 25 March 2024, date last accessed).
- Engineers Edge. *Pipe Roughness Coefficients Table Charts*. https://www.engineersedge.com/fluid_flow/pipe-roughness.htm. (18 April 2024, date last accessed).
- Massey BS. *Mechanics of Fluids*. 6th ed. London: Chapman & Hall, 1992.
- Carlsaw HS, Jaeger JC. *Conduction of Heat in Solids*. 2nd ed. London: Oxford University Press, 1959.
- Nian YL, Cheng WL. Insights into geothermal utilization of abandoned oil and gas Wells. *Renew Sust Energy Rev* 2018;87:44–60. <https://doi.org/10.1016/j.rser.2018.02.004>.
- Li M, Lai ACK. Review of analytical models for heat transfer by vertical ground heat exchangers (GHEs): a perspective of time and space scales. *Appl Energy* 2015;151:178–91. <https://doi.org/10.1016/j.apenergy.2015.04.070>.
- Ingersoll LR, Zobel OJ, Ingersoll AC. *Heat Conduction with Engineering, Geological and Other Applications*. New York: McGraw-Hill Book Company, 1948.
- Srimannarayana VV, Kumar MSSM, Siddharth GP. *et al.* Interpretation of radius of investigation in composite reservoir. *J Emerg Technol Innov Res* 2014;10:234–72.
- Colebrook CF. Turbulent flow in pipes, with particular reference to the transition region between the smooth and rough pipe Laws. *J Inst Civ Eng* 1939;11:133–56. <https://doi.org/10.1680/jiote.1939.13150>.
- Gnielinski V. Neue Gleichungen für den Wärme- und den Stoffübergang in turbulent durchströmten Rohren und Kanälen [new equations for heat and mass transfer in turbulent flow tubes and channels]. *Forsch Ingenieurwes A* 1975;41:8–16. <https://doi.org/10.1007/BF02559682>.
- Nalla G, Shook GM, Mines GL. *et al.* Parametric sensitivity study of operating and design variables in wellbore heat exchangers. *Geothermics* 2005;34:330–46. <https://doi.org/10.1016/j.geothermics.2005.02.001>.
- American Petroleum Institute, ISO 11960:2004. *Specification for Casing and Tubing. API Specification 5CT. Petroleum and Natural Gas Industries – Steel Pipes for Use as Casing or Tubing Wells*. 8th ed. Washington, D.C.: API Publishing Services, 2004.
- Kubačka J, Tyacke J, Pittman I. *et al.* Energy availability from deep geothermal wells using coaxial heat exchangers. In: Riffat S. (ed.) *Sustainable Energy Technologies 2022: Proceedings of the 19th International Conference on Sustainable Energy Technologies*, 16th–18th August 2022, Istanbul, Turkey. University of Nottingham: Buildings, Energy & Environment Research Group; 2022, 28–38.